J. Shanghai Jiao Tong Univ. (Sci.), 2018, 23(1): 202-208
https://doi.org/10.1007/s12204-018-1926-9

Electronic Structure and Stability of Lead-free Hybrid Halide Perovskites: A Density Functional Theory Study

WU Jiayi[a] (邬嘉义), *QI Wen*[a] (戚 文), *LUO Zhe*[b] (罗 哲), *LIU Ke*[a] (刘 科), *ZHU Hong*[a,c*] (朱 虹)
(a. University of Michigan - Shanghai Jiao Tong University Joint Institute; b. National Engineering Research Center of Light Alloys; c. Materials Genome Initiative Center, Shanghai Jiao Tong University, Shanghai 200240, China)

Abstract: The most commonly used and studied hybrid halide perovskite is ABX_3, where A usually stands for CH_3NH_3, B for Pb, and X for I. A lead-free perovskite with high stability and ideal electronic band structure would be of essence, especially considering the toxicity of lead. In this work, we have considered 11 metal elements for the B site and three halide elements (Cl, Br, and I) including various combinations among the three halides for the X site. A total number of 99 hybrid perovskites are studied to understand how the crystal structure, band gap and stability can be tuned by the chemistry modification, i.e., the replacement of toxic element, Pb in the original $MAPbX_3$, with non-toxic metal elements. We find that the favorable substitutes for Pb in $MAPbI_3$ are Ge and Sn.

Key words: hybrid halide perovskites, band gap, phase stability, density functional theory (DFT)
CLC number: O 469 **Document code:** A

0 Introduction

Hybrid halide perovskites have experienced a rapid development as efficient photon-absorption materials in solar cells since 2009. They possess a high carrier mobility, proper band gap and simplicity of fabrication, which are key factors for photovoltaic devices. Among the hybrid halide perovskites, methylammonium lead halide ($MAPbX_3$) is the one that attains a lot of research interest with the highest reported power conversion efficiency 20.1%[1-2], where MA is methylammonium. Although the band gap of $MAPbX_3$ is found to be close to the ideal band gap of 1.34 eV according to Shockley-Queisser limit under the air-mass (AM) of 1.5 solar spectrum[3], lead is a toxic element to both human being and the environment. Thus, the development of a non-toxic perovskite material with proper band gap and stability is one of the major targets throughout this field. A theoretical understanding about how the electronic properties may change with the replacement of toxic Pb in the original $MAPbX_3$ with non-toxic metal elements appears extremely important.

The crystal structure of cubic $MABX_3$ is shown in the next section. Although perovskites can also form other crystal structures under different pressure and temperature (such as monoclinic, tetragonal, and orthorhombic phases), $MAPbX_3$(X = Cl, Br, I) may undergo a series of phase transitions from orthorhombic to tetragonal and then from tetragonal to cubic, which occur at 161.4 and 330.4 K[4] respectively for $MAPbI_3$. Considering that the solar cell is operated at room temperature and cubic structure ensures a higher degree of ionic bonding and thus provides optimum electronic properties[5], we focus on the stability, electronic property and crystal structures of cubic phase lead-free $MABX_3$ in this work.

It has been reported that the band gap of perovskites varies with the element at the B site and is also dependent on the halide elements at the X site. Kulkarni et al.[6] studied the band gap of mixed halide perovskite $MAPbI_{3-3x}Br_{3x}$ and found that the band gap increased with the addition of Br which had a smaller atomic radius compared with iodine. Kitazawa et al.[7] studied the band gap of $CH_3NH_3PbI_{3-x}Cl_x$ and found that the band gap increased with the addition of Cl and the band gap for $MAPbCl_3$ is 3.11 eV. Apart from the band gaps, stability is another major issue concerning hybrid perovskites. The organic-inorganic lead perovskites, e.g., $MAPbX_3$, are reported to undergo a degradation process after a long-term usage, mostly due to high temperature and moisture. $MABX_3$ tends to decompose to MAX and BX_2, where the

Received date: 2017-12-14
Foundation item: the Shanghai Sailing (YANG FAN) Program (No. 16YF1406000), and the Startup Fund from Shanghai Jiao Tong University
Author contributions: WU Jiayi and QI Wen contributed equally to this work.
∗**E-mail:** hong.zhu@sjtu.edu.cn

reaction can be described as $MABX_3 \rightarrow MAX + BX_2$. Although some efforts have been put on the modification of $MAPbI_3$ either through modifying the B site elements or through tuning the X site elements[8], a systematic understanding about the joint effect of B and X site element replacement on structure, stability and electronic property is still lacked but important for the design of lead-free perovskite materials for photon absorption.

In this work, we use high-throughput calculations based on density functional theory (DFT) for 99 $MABX_3$ perovskites. For B site substitution, we choose all metal elements that show +2 valences in the periodic table for the completeness. In this scheme, B can be Be, Mg, Ca, Sr, Ba, Zn, Cd, Hg, Ge, Sn or Pb; X_3 can be various combinations of halide elements, including Cl_3, Br_3, I_3, I_2Br, I_2Cl, IBr_2, ICl_2, $ClBr_2$ and $BrCl_2$. We note that Be, Hg and Cd are toxic elements and the hybrid perovskites made of these elements may not be appropriate alternatives to $MAPbI_3$ for the real application. The results of band gap calculation, stability analysis and toxicity show that the possible replacement of $MAPbI_3$ falls into the ones with Ge and Sn which have proper band gaps and are equally or even more stable than $MAPbI_3$.

1 Methodology

The DFT calculations are performed in the Vienna ab initio simulation package (VASP) with the Perdew-Burke-Ernzerhof (PBE) generalized gradient approximation (GGA) and projector augmented-wave (PAW) pseudopotentials[9-11]. All calculations are performed with a cut-off energy of 520 eV and a Monkhorst k-point mesh of $4 \times 4 \times 4$. The energy convergence of the calculated system is 6×10^{-4} eV. The relaxed lattice parameters for $MAPbI_3$ are calculated to be $a = 645.73(1)$ μm, $b = 645.75(1)$ μm, $c = 645.74(9)$ μm, which agree well with the experimental value of $a = 627.6(4)$ μm[12]. Our high-throughput computations on the structure optimizations and electronic structure calculations for 99 perovskite materials are realized based on pymatgen (a robust materials analysis code)[13], FireWorks (an open-source code for defining, managing, and executing individual calculation tasks)[14] and the whole workflow and Custodian (a simple, robust and flexible just-in-time job management framework in Python). For those compounds with a determined GGA band gap between 0.5—2.0 eV, we also perform beyond-conventional DFT calculations using Heyd-Scuseria-Ernzerhof (HSE) functional (i.e., HSE06) to get a more accurate determination of the band gaps[15-16]. The crystal structure of cubic $MABX_3$ is shown in Fig. 1, where MA molecule takes the corner position, the metal element B takes the body center position, and the halide element X takes the face center position.

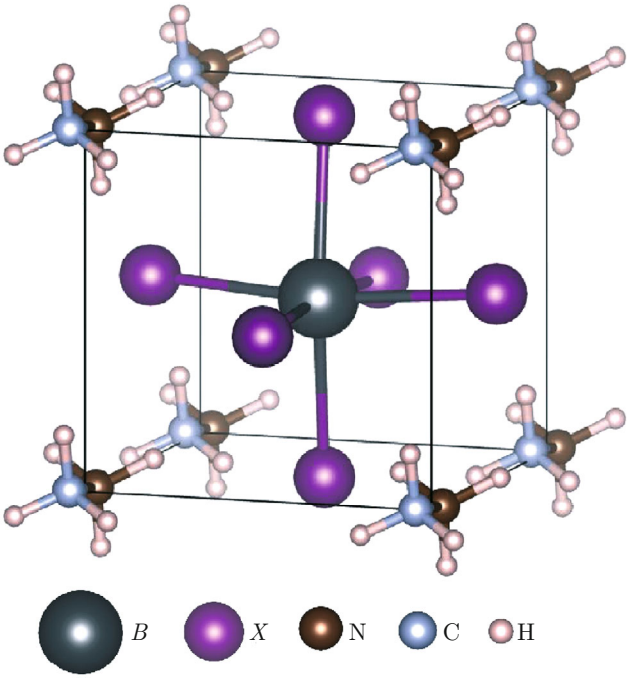

Fig. 1 The crystal structure of cubic perovskite $MABX_3$

2 Band Gap of $MABX_3$

The GGA band structure of $MAPbI_3$ along the high symmetry k-path is shown in Fig. 2, where E is the energy and E_F represents Fermi level. The sizes of purple dots in Figs. 2(a) and 2(b) represent the characters of Pb and I, respectively; the red and green dots at B|Z indicate the conduction band minimum (CBM) and valence band maximum (VBM), respectively. The CBM and VBM occur at the same reciprocal point, which indicates that $MAPbI_3$ is a direct band gap material. The element projected band structure and orbital projected density of states (DOS) clearly show that the CBM is mostly contributed by Pb-p orbital, and the VBM is contributed mostly by the I-p and Pb-s hybrid orbitals, like the findings from Yuan et al[17].

The calculated GGA band gaps for all the 99 perovskites considered in this work are shown in Fig. 3. The GGA band gaps usually range from 0.4 to 5.2 eV, except for $MACdCl_3$, $MAHgCl_3$, $MAHgBr_3$ and $MAHgI_3$ with a zero band gap. According to the Shockley-Queisser limit, the optimum band gap for single-junction solar cell is 1.34 eV under AM of 1.5 solar spectrum with the highest efficiency 33.7%, while the silicon based solar cells have less favorable band gap of 1.1 eV but a maximum efficiency of 32%[18]. Thus, the band gap of 1.0—1.7 eV is defined to be the proper band gap region for photon absorption in our calculations[19]. It can also be seen that the band gap of $MABX_3$ with B = Ge, Sn and Pb falls into the optimum range, suggesting that Ge, Sn and Pb are the

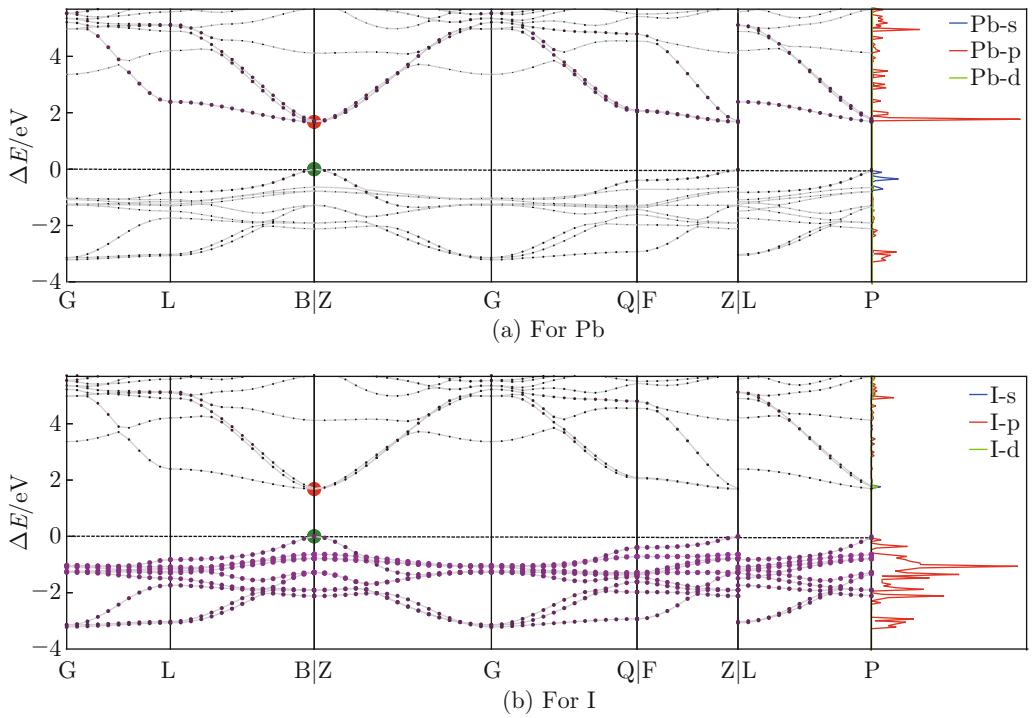

Fig. 2 Element projected band structure and orbital projected DOS of $MAPbI_3$ ($\Delta E = E - E_F$)

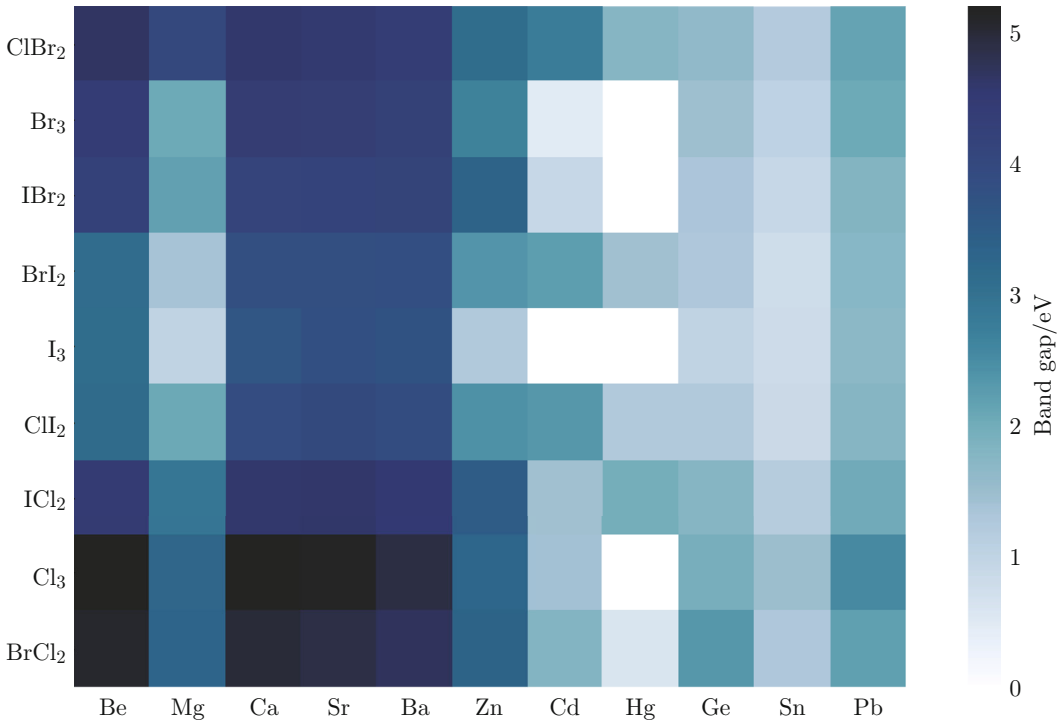

Fig. 3 GGA band gaps of $MABX_3$ with B = Be, Mg, Ca, Sr, Ba, Zn, Cd, Hg, Ge, Sn, Pb and X_3 = $ClBr_2$, Br_3, IBr_2, BrI_2, I_3, ClI_2, ICl_2, Cl_3, $BrCl_2$ in the unit of eV

top three metal elements suitable for photovoltaic perovskites. As shown in Fig. 3, the ones with alkali earth metals and Zn are usually not appropriate for alternatives to $MAPbI_3$, since the GGA band gaps of almost all the combinations of halide elements are beyond the optimum band gap region.

For the lead-based perovskite $MAPbX_3$, we find if the iodine element is involved, the calculated GGA

band gaps will be within the 1—2 eV region, which may explain why iodine-based lead halide perovskites are reported to be good light absorption materials. The comparison of the band gaps for MABI$_3$, MABClI$_2$, MABCl$_2$I and MABCl$_3$ reveals that the addition of iodine will reduce the band gap. The band gaps of MABX_3 increase when X changes from I, Br to Cl for most cases, which indicates that Cl can be used to tune up the band gap, while the tuning down of the band gap may be attributed to I, in agreement with prior reports[20]. Since these halide elements all have the same valence electrons, the major difference may derive from the electronegativity difference. Here we know the electronegativity of the three halide elements in the Mulliken's scale: $\chi_{\mathrm{Cl}} = 8.30\,\mathrm{eV}$, $\chi_{\mathrm{Br}} = 7.5\,\mathrm{eV}$, $\chi_{\mathrm{I}} = 6.7\,\mathrm{eV}$, and the combined electronegativity can be expressed as $(\chi_{\mathrm{Cl}}\chi_{\mathrm{Br}}\chi_{\mathrm{I}})^{1/3}$ for the combination of ClBrI. We find that the band gaps increase with the increase of the combined electronegativity, like Ivano's findings[21]. In addition, considering the radius of the halide elements, $r_{\mathrm{Cl}} = 79\,\mathrm{pm}$, $r_{\mathrm{Br}} = 94\,\mathrm{pm}$, $r_{\mathrm{I}} = 115\,\mathrm{pm}$, we find that larger halide element in X site will result in a smaller band gap. Band gap can be further correlated to crystal structure volume. Figure 4 illustrates the volume for the unit cell of all the 99 perovskites. For each column in the volume plot, the perovskites in the center of each column are larger in volume. However, for the band gap plot, the energy gaps in the center of each column are smaller than the ones in the outside region. This indicates that for perovskites with the same metal element, the larger the volume is, the smaller the band gap appears to be. We find that the iodine-based perovskites have a larger volume but smaller band gap, which may be explained by the larger atomic radius of iodine among the three halide elements considered in this work.

Considering that the band gap calculated by GGA functional is usually underestimated[22], we go beyond standard DFT and use hybrid functional for the perovskites with the GGA band gap in a range of 0.5—2 eV, which combines the electron correlation energy in GGA with the exact exchange energy from Hartree-Fock. As Table 1 shows, the HSE band gap is overall larger than the GGA values. We find the MASnI$_3$ HSE band gap of 1.04 eV is in a much better agreement with the experimental value of 1.2 eV[23], compared with the GGA band gap of 0.74 eV. Even for light metal elements, HSE functional predicts the band gap in better agreement with the experimental values. For perovskite with heavy elements in B site, the GGA band gap is in a better agreement with the experimental values. For example, GGA band gap of MAPbI$_3$ is 1.54 eV compared with the experimental value of 1.56 eV[6], which is much smaller than the HSE band gap of 2.11 eV. This is mainly due to the neglect of spin-orbit coupling which lowers the band gap. Thus for non-Pb and Pb-based perovskites, we are especially interested in HSE band gap and GGA band gap, respectively, in 1.0—1.7 eV. Those compounds with proper band gaps in this range are labeled with textboxes in Table 1.

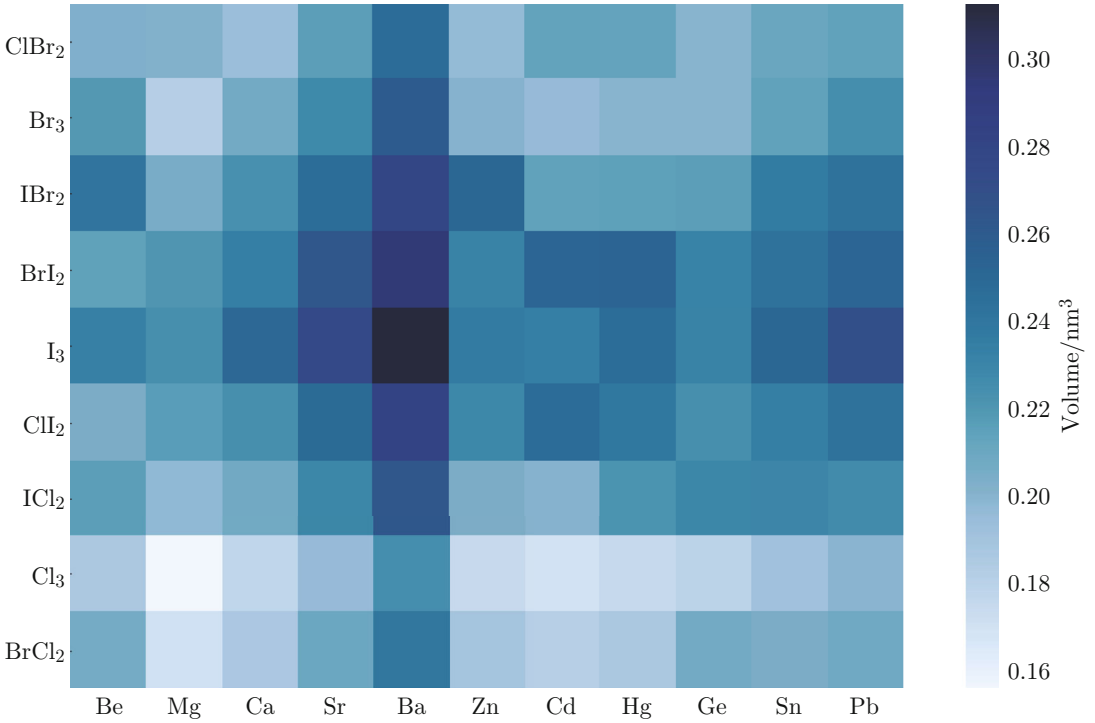

Fig. 4 Volume for the unit cell of all the 99 perovskites

Table 1 The calculated GGA and HSE band gaps of $MABX_3$

Compound	Band gap/eV		Compound	Band gap/eV	
	HSE	GGA		HSE	GGA
$MACdBrCl_2$	3.09	1.79	$MAGeI_2Cl$	1.65	1.22
$MACdICl_2$	2.54	1.40	$MAGeICl_2$	2.34	1.75
$MACdCl_3$	2.82	1.39	$MAGeCl_3$	2.68	1.93
$MACdIBr_2$	1.92	0.88	$MAGeI_3$	1.61	1.19
$MASnBrCl_2$	1.83	1.29	$MAPbIBr_2$	2.36	1.79
$MASnBr_2Cl$	1.25	1.19	$MAPbI_2Br$	2.20	1.69
$MASnBr_3$	1.31	1.01	$MAPbI_2Cl$	2.59	1.72
$MASnICl_2$	1.62	1.15	$MAPbICl_2$	2.34	1.98
$MASnCl_3$	2.25	1.63	$MAPbI_3$	2.11	1.54 (1.57)[21]
$MASnI_2Cl$	1.16	0.80	$MAHgBr_2Cl$	2.83	1.73
$MASnI_3$	1.04	0.74(1.20)[24]	$MAHgI_2Br$	2.29	1.40
$MASnIBr_2$	1.30	0.89	$MAHgI_2Cl$	2.13	1.95
$MASnI_2Br$	1.09	0.75	$MAHgICl_2$	2.99	1.25
$MAGeBr_2Cl$	2.26	1.62	$MAHgBrCl_2$	1.58	0.60
$MAGeCl_2Br$	1.93	1.36	$MAMgI_2Br$	2.24	1.35
$MAGeIBr_2$	1.85	1.26	$MAMgI_3$	1.82	0.97
$MAGeBr_3$	2.07	1.46	$MAZnI_3$	3.15	2.10

Note: those compounds with proper band gaps are in textbox; the corresponding experimental values are in parentheses.

3 Stability Analysis of $MABX_3$

The stability of the perovskites can be evaluated via their energy above hull. The energy above hull[25] represents the energy of the decomposition reaction of one material into all possible stable combinations of compounds and elementary substances. With all the potential chemical combinations as references, stability can be evaluated. For example, a $CaTiO_3$ is tested with respect to all the other $CaTiO_3$ with different crystal structures, CaO and TiO_2 mixtures, and Ca, Ti, O_2 mixtures. A positive value of energy above hull indicates that the material is instable as compared with the references, while the stable material has a zero energy above hull.

Perovskite $MAPbI_3$ will be stable in cubic phase above 327.4 K according to experiment and calculations[26]. Tetragonal phase can be maintained between 162.2 and 327 K, which transforms to orthorhombic structure at low temperature[27]. Since our calculations of cubic phase are performed at 0 K, we examine all the possible compounds that the perovskite may decompose to, and the corresponding decomposition process follows

$$\mathrm{MAB}X_3 \rightarrow BX_2 + \mathrm{CH_2} + \mathrm{NH_4}X. \tag{1}$$

The energy above hull plot is illustrated in Fig. 5, from which we note that Ge, Sn and Pb are the top three B site elements with the lowest energy above hull. Sn-based perovskites appear to be the most stable ones, considering that all the materials with Sn have a lower energy above hull as compared with $MAPbI_3$. On the other hand, the high energy above hull values of Mg-based perovskite indicates that Mg-based perovskites are the least stable ones. It is shown that for the hybrid perovskite involving Pb, the stability descends in order of Cl, Br and I in agreement with prior reports[21].

The stability of perovskites is further analyzed based on the formation energy of $MABX_3$ from MAX and BX_2, which is defined as

$$E_\mathrm{f} = E_{\mathrm{MA}X} + E_{BX_2} - E_{\mathrm{MA}BX_3}, \tag{2}$$

where E_f represents the formation energy to form the perovskite from compounds MAX and BX_2 and a positive value means that the compound $MABX_3$ is stable, $E_{\mathrm{MA}X}$ is the formation energy of MAX, E_{BX_2} stands for the formation energy of BX_2, and $E_{\mathrm{MA}BX_3}$ represents the formation energy of $MABX_3$. The materials with higher formation energy possess better stability. As shown in Fig. 6, the iodine-based perovskites with high formation energy are $MASnI_3$, $MAZnI_3$, and $MASrI_3$.

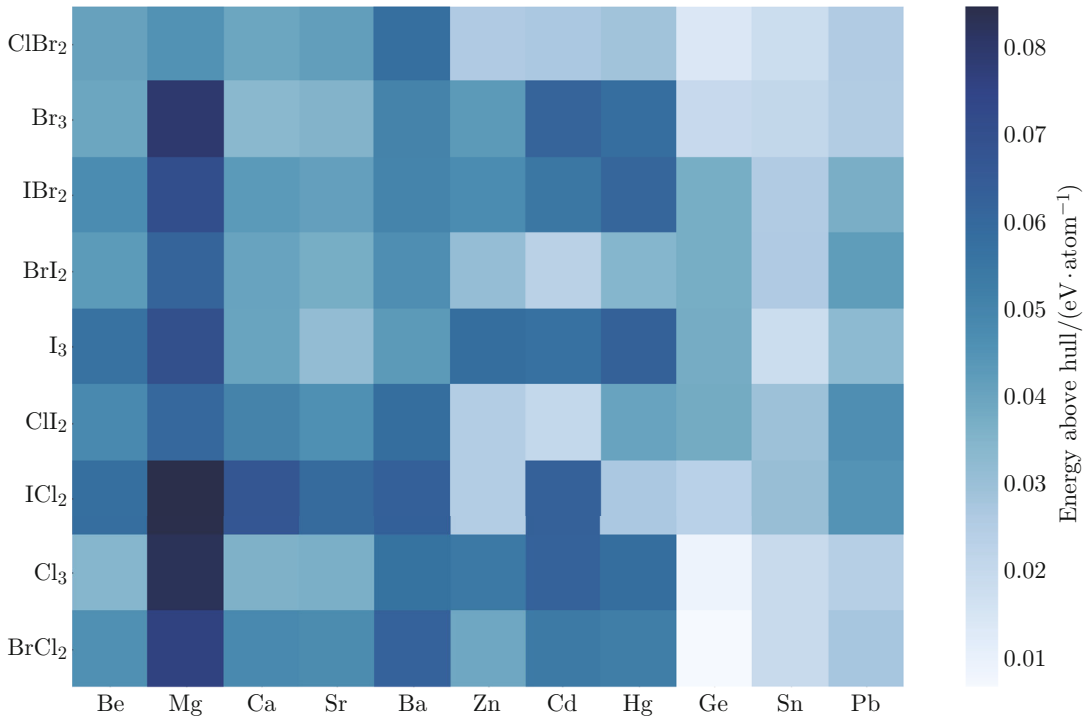

Fig. 5 The energy above hull plot for all the 99 halide perovskites considered in this work

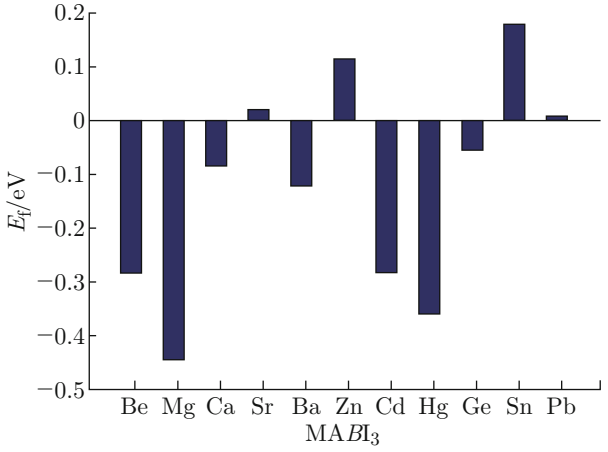

Fig. 6 Formation energy of MABI$_3$ with B = Be, Mg, Ca, Sr, Ba, Zn, Cd, Hg, Ge, Sn, Pb

4 Conclusion

In this work, 99 potential alternatives to MAPbI$_3$ have been studied by the DFT calculations to get a comprehensive understanding on how metal elements at B sites and halide elements at X sites affect the structure, electronic property and stability, which may be useful for the development of lead-free perovskite materials. The results of band gap calculation and the stability analysis show that the possible replacement of MAPbI$_3$ falls into the ones with Ge and Sn. The hybrid perovskites with these metals involved have the band gaps within the proper region and most of the ones with Sn and Ge are found to be equally or more stable than MAPbI$_3$. Besides, perovskites with alkali earth metals fail to meet either criterion. It is also found that the band gap as well as the stability can be further modified through a proper combination of the halide elements as well as B site element. For example, MAGeIBr$_2$ has a band gap of 1.85 eV and an energy above hull of 0.045 eV/atom, while MAPbI$_2$Cl has a band gap of 1.65 eV and an energy above hull of 0.042 eV/atom.

Acknowledgement The authors also thank the computing resources from Shanghai Jiao Tong University Supercomputer Center.

References

[1] NOH J H, IM S H, HEO J H, et al. Chemical management for colorful, efficient, and stable inorganic-organic hybrid nanostructured solar cells [J]. *Nano Letters*, 2013, **13**(4): 1764-1769.

[2] ZHOU H, CHEN Q, LI G, et al. Interface engineering of highly efficient perovskite solar cells [J]. *Science*, 2014, **345**(6196): 542-546.

[3] SHOCKLEY W, QUEISSER H J. Detailed balance limit of efficiency of p-n junction solar cells [J]. *Journal of Applied Physics*, 1961, **32**(3): 510-519.

[4] BAIKIE T, BARROW N S, FANG Y, et al. A combined single crystal neutron/X-ray diffraction and

solid-state nuclear magnetic resonance study of the hybrid perovskites $CH_3NH_3PbX_3$ (X = I, Br and Cl) [J]. *Journal of Materials Chemistry A*, 2015, **3**: 9298-9307.

[5] CHEN Q, MARCO N D, YANG Y, et al. Under the spotlight: The organic-inorganic hybrid halide perovskite for optoelectronic applications [J]. *Nano Today*, 2015, **10**(3): 355-396.

[6] KULKARNI S A, BAIKIE T, BOIX P P, et al. Band-gap tuning of lead halide perovskites using a sequential deposition process [J]. *Journal of Materials Chemistry A*, 2014, **2**: 9221-9225.

[7] KITAZAWA N, WATANABE Y, NAKAMURA Y. Optical properties of $CH_3NH_3PbX_3$ (X = halogen) and their mixed-halide crystals [J]. *Journal of Materials Science*, 2012, **37**(17): 3585-3587.

[8] MCMEEKIN D P, SADOUGHI G, REHMAN W, et al. A mixed-cation lead mixed-halide perovskite absorber for tandem solar cells [J]. *Science*, 2016, **351**(6269): 151-155.

[9] KRESSE G, FURTHMULLER J. Efficient iterative schemes for ab initio total-energy calculations using a plane-wave basis set [J]. *Physical Review B*, 1996, **54**(16): 11169-11186.

[10] PERDEW J P, BURKE K, ERNZERHOF M. Generalized gradient approximation made simple [J]. *Physical Review Letters*, 1996, **77**(18): 3865-3868.

[11] KRESSE G, JOUBERT D. From ultra-soft pseudopotentials to the projector augmented-wave method [J]. *Physical Review B*, 1999, **59**(3): 1758-1775.

[12] TOM B, YANAN F, JEANNETTE M K, et al. Synthesis and crystal chemistry of the hybrid perovskite $(CH_3NH_3)PbI_3$ for solid-state sensitised solar cell applications [J]. *Journal of Materials Chemistry A*, 2013, **1**: 5628-5641.

[13] ONG S P, RICHARDS W D, JAIN A, et al. Python materials genomics (pymatgen): A robust, open-source Python library for materials analysis [J]. *Computational Materials Science*, 2013, **68**: 314-319.

[14] MATHEW K, SINGH A K, GABRIEL J J, et al. MP interfaces: A materials project based Python tool for high-throughput computational screening of interfacial systems [J]. *Computational Materials Science*, 2016, **122**: 183-190.

[15] HEYD J, SCUSERIA G E, ERNZERHOF M. Hybrid functionals based on a screened coulomb potential [J]. *The Journal of Chemical Physics*, 2003, **118**(18): 8207-8215.

[16] PAIER J, MARSMAN M, HUMMER K, et al. Screened hybrid density functionals applied to solids [J]. *The Journal of Chemical Physics*, 2006, **124**(15): 154709.

[17] YUAN Y, XU R, XU H T, et al. Nature of the band gap of halide perovskites ABX_3 (A = CH3NH3, Cs; B = Sn, Pb; X = Cl, Br, I): First-principles calculations [J]. *Chinese Physics B*, 2015, **24**(11): 116302.

[18] RÜHLE S. Tabulated values of the Shockley-Queisser limit for single junction solar cells [J]. *Solar Energy*, 2016, **130**:139 -147.

[19] PAUWELS H, DE VOS A. Determination of the maximum efficiency solar cell structure [J]. *Solid-State Electronics*, 1981, **24**(9): 835-843.

[20] KRESSE G, FURTHMLLER J. Efficiency of ab-initio total energy calculations for metals and semiconductors using a plane-wave basis set [J]. *Computational Materials Science*, 1996, **6**(1): 15-50.

[21] CASTELLI I E, GARCÍA-LASTRA J M, THYGESEN K S, et al. Bandgap calculations and trends of organometal halide perovskites [J]. *APL Materials*, 2014, **2**(8): 081514.

[22] CHEN T, FOLEY B J, IPEK B, et al. Rotational dynamics of organic cations in the $CH_3NH_3PbI_3$ perovskite [J]. *Physical Chemistry Chemical Physics*, 2015, **17**: 31278-31286.

[23] UMARI P, MOSCONI E, ANGELIS E D. Relativistic GW calculations on $CH_3NH_3PbI_3$ and $CH_3NH_3SnI_3$ perovskites for solar cell applications [J]. *Scientific Reports*, 2014, **4**: 4467.

[24] LIU M, RONG Z Q, MALIK R, et al. Spinel compounds as multivalent battery cathodes: A systematic evaluation based on ab initio calculations [J]. *Energy & Environmental Science*, 2015, **8**(3): 964-974.

[25] OKU T. Crystal structures of $CH_3NH_3PbI_3$ and related perovskite compounds used for solar cells [C]//*Solar Cells-New Approaches and Reviews*. Rijeka: InTech, 2015: 77-101.

[26] CONINGS B, DRIJKONINGEN J, GAUQUELIN N, et al. Intrinsic thermal instability of methylammonium lead trihalide perovskite [J]. *Advanced Energy Materials*, 2015, **5**(15): 1500477.